Published in final edited form as:
Cancer Res. 2013 July 15; 73(14): 4439–4450. doi:10.1158/0008-5472.CAN-13-0187.

Antitumor Activity of a Humanized, Bivalent Immunotoxin Targeting Fn14-Positive Solid Tumors

Hong Zhou[1], **Walter N. Hittelman**[1], **Hideo Yagita**[2], **Lawrence H. Cheung**[1], **Stuart S. Martin**[3], **Jeffrey A. Winkles**[4,*], and **Michael G. Rosenblum**[1,*]

[1]Department of Experimental Therapeutics, UT M.D. Anderson Cancer Center, Houston, TX, 77030

[2]Department of Immunology, Juntendo University School of Medicine, Tokyo, Japan

[3]Department of Physiology, Marlene and Stewart Greenebaum Cancer Center, University of Maryland School of Medicine, Baltimore, MD, 21201

[4]Department of Surgery, Center for Vascular and Inflammatory Diseases, and the Marlene and Stewart Greenebaum Cancer Center, University of Maryland School of Medicine, Baltimore, MD, 21201

Abstract

The TWEAK (TNFSF12) receptor Fn14 (TNFRSF12A) is expressed at low levels in normal tissues but frequently highly expressed in a wide range of tumor types such as lung, melanoma, and breast and therefore it is a potentially unique therapeutic target for these diverse tumor types. We have generated a recombinant protein containing a humanized, dimeric single-chain anti-Fn14 antibody fused to recombinant gelonin toxin as a potential therapeutic agent (designated hSGZ). The hSGZ immunotoxin is a highly potent and selective agent that kills Fn14-positive tumor cells *in vitro*. Treatment of cells expressing the multidrug resistance protein MDR1 (ABCB1B) showed no cross-resistance to hSGZ. Induced overexpression of Fn14 levels in MCF7 cells through HER2 (ERBB2) signaling translated to an improved therapeutic index of hSGZ treatment. In combination with trastuzumab, hSGZ demonstrated an additive or synergistic cytotoxic effect on HER2+/Fn14+ breast cancer cell lines. Also, hSGZ treatment inhibited Erb3/Akt signaling in HER2-overexpressing breast cancer cells. Pharmacokinetic studies in mice revealed that hSGZ exhibited a bi-exponential clearance from plasma with a rapid initial clearance ($t_{1/2\,\alpha}$ = 1.26 h) followed by a 7-fold longer plasma half life ($t_{1/2\,\beta}$ = 7.29 h). At 24, 48 and 72 h after injection, uptake of the hSGZ into tumors was 5.1, 4.8 and 4.7 %ID/g, with a tumor-to-muscle ratio of 5.6, 6.2 and 9.0, respectively. Therapeutic efficacy studies showed significant tumor inhibition effects using an MDA-MB-231/Luc breast cancer xenograft model. Our findings show that hSGZ is an effective anticancer agent and a potential candidate for clinical studies.

Keywords

Fn14; immunotoxin; hSGZ

Correspondence to: Michael G. Rosenblum, Ph.D., Department of Experimental Therapeutics, M. D. Anderson Cancer Center, Unit 1950, 1515, Holcombe Boulevard, Houston, TX, 77030, mrosenbl@mdanderson.org; Phone: 713-792-3554, Jeffrey A. Winkles, Ph.D., Department of Surgery, 800 West Baltimore Street, Room 320, University of Maryland School of Medicine, Baltimore, MD, 21201, jwinkles@som.umaryland.edu; Phone: 410-706-8172; FAX: 410-706-8234.
*Co-Corresponding Authors.

Conflict of interest: None

Introduction

Breast cancer remains the leading cause of cancer death in females worldwide (1). Despite the robust clinical efficacy of trastuzumab (Herceptin) in HER2-positive breast cancer, primary and secondary resistance is frequently encountered (2). Inherent tumor heterogeneity and upregulation of alternative survival pathways in tumor cells frequently lead to emergence of resistance and treatment failure. Triple-negative breast cancer (TNBC) is a subtype of breast cancer distinguished by the absence of three critical regulatory receptors: estrogen, progesterone and HER2. These breast tumors generally display a more aggressive clinical course exacerbated by the lack of effective targeted therapies (3). There is a significant need to identify new targets and treatment approaches to overcome or suppress the emergence of resistance. Thus, translational studies to develop novel targeted therapeutics remains a clinical imperative.

Fibroblast growth factor-inducible 14 kDa protein (Fn14) is the cell surface receptor for the cytokine TNF-like weak inducer of apoptosis (TWEAK) (4). This receptor has been proposed as a novel target for cancer therapy because of its strong overexpression in many types of solid tumors and the intrinsic tumor cell killing capacity of the TWEAK-Fn14 pathway (5–7). TWEAK triggers multiple cellular responses including proliferation, migration, differentiation, apoptosis, angiogenesis and inflammation through its cognate receptor Fn14 (5, 6). TWEAK-dependent Fn14 signalling can exert either pro-tumorigenic (8) or antitumorigenic (9, 10) effects depending on the particular microenvironmental conditions *in vivo* (6). TWEAK-independent Fn14 signalling may promote tumor cell invasion and metastasis (6).

The Fn14 receptor is expressed at relatively low levels in normal tissues, but is dramatically elevated in a wide variety of human tumor types (11–21) and also can be expressed by tumor stroma and vasculature (5, 22). The correlation between increased Fn14 expression and higher tumor grade and/or poor prognosis has been documented in glioma (12, 13), breast cancer (14, 23), esophageal cancer (15, 16), prostate cancer (17), gastric cancer (18) and bladder cancer (19).

Two types of Fn14-targeted agents have been tested in preclinical cancer studies - agonist antibodies (10, 11, 23, 24) and immunotoxins (21, 25). Our group showed that an immunoconjugate designated ITEM4-rGel composed of a murine mAb targeting the Fn14 receptor and the recombinant toxin gelonin was highly efficacious in inhibiting tumor growth *in vivo* (25). To develop an Fn14-targeted immunotoxin more suitable for clinical use, we generated a humanized, dimeric single-chain ITEM-4 construct fused to rGel (designated hSGZ) (21). The hSGZ construct was shown to rapidly internalize and deliver the rGel payload to the cytosol of tumor cells where it enzymatically blocks protein synthesis. We previously demonstrated that hSGZ binds to the external domain of Fn14 with high affinity (K_d ~ 1.4 nmol/L) and induces necrosis in Fn14-positive melanoma target cells (21). In addition, treatment of melanoma cells with the hSGZ construct up-regulated cellular Fn14 expression and triggered cell signaling events similar to the Fn14 ligand TWEAK. Administration of hSGZ also showed excellent efficacy in a melanoma xenograft model (21).

In the current study, we examined the efficacy of the hSGZ construct against breast tumor cell lines and examined hSGZ in combination with trastuzumab on HER2+ and Fn14+ breast tumor cell lines. Some lines demonstrated either an additive or a synergistic cytotoxic effect. In addition, we found that breast tumor cells resistant to chemotherapeutic agents were not significantly cross-resistant to hSGZ. Targeting Fn14 by hSGZ resulted in inhibition of Erb3/Akt signaling pathway in HER2-overexpressing breast cancer cells. We

further examined the *in vitro* and *in vivo* efficacy of hSGZ on breast cancer cells and the pharmacokinetics and biodistribution of hSGZ in mice. These findings support the proposal that Fn14 is a potential therapeutic target for both HER2+ and triple-negative breast cancer as well as other Fn14 over-expressing tumors such as melanoma and warrant the clinical investigation of hSGZ as a novel, targeted agent for these cancer subtypes.

Materials and Methods

Cell lines and reagents

Human breast cancer cell lines MDA-MB-231, MCF-7, eB1, BT-474, and SKBR3 were maintained in RPMI 1640 medium. MCF7/HER2 cells were provided by Dr. Dihua Yu (MD Anderson Cancer Center). The stable luciferase-expressing line MDA-MB-231/Luc was generated and grown as described previously (26). Fn14-deficient mouse embryonic fibroblasts (MEF 3.5−/−) were maintained in DMEM. All media contain 10% fetal bovine serum. The multidrug-resistant (MDR) (P-gp–overexpressing) human melanoma cell line MDA-MB-435/LCC6^{MDR1} was established as previously described (27). The human ovarian cancer cell line HeyA8 and its multidrug-resistant equivalent HeyA8-MDR were maintained as previously described (28).

Cell lines (MCF-7, BT-474, SKBR3 and MDA-MB-231) were validated by STR DNA fingerprinting using the AmpFℓSTR Identifiler kit according to manufacturer instructions (Applied Biosystems). The STR profiles were compared to known ATCC fingerprints (ATCC.org), to the Cell Line Integrated Molecular Authentication database (CLIMA) version 0.1.200808 (http://bioinformatics.istge.it/clima/) (Nucleic Acids Research 37:D925-D932 PMCID: PMC2686526) and to the MD Anderson fingerprint database. The STR profiles matched known DNA fingerprints or were unique. No additional authentication was done for other transformed cell lines in this study.

The murine IgG2b/κ monoclonal antibody ITEM-4 directed against human and mouse Fn14 receptor (29) and the generation of immunoconjugate ITEM4-rGel have been described previously (25). hSGZ was expressed in the soluble fraction of *Escherichia coli* and purified to homogeneity after two chromatographic steps: cobalt affinity and ion exchange (21). The HER2-specific mAb trastuzumab (Herceptin) was manufactured by Genentech and purchased from the MD Anderson Cancer Center Pharmacy. D-Luciferin (sodium salt) was purchased from Gold Biotechnology, Inc.

In vitro cytotoxicity assays

Cell viability was determined using the crystal violet staining method followed by solubilization of the dye in Sorensor's buffer as described previously (25).

Lactate dehydrogenase (LDH) release assay

LDH was measured using LDH Cytotoxicity Detection Kit from Clontech Laboratories, Inc. (Mountain View, CA) according to manufacturer’s instructions.

Internalization analysis

Immunofluorescence-based internalization studies were done on MDA-MB-231 and MEF 3.5−/− cells as described previously (25).

Flow cytometry analysis for Fn14 cell surface expression

Flow cytometry analysis of cells stained with ITEM-4 was performed as described previously (25).

Western blot analysis

Western blots were performed according to standard procedures. Antibodies used include phosphorylated HER2, HER2, phosphorylated ErbB-3 (Tyr 1328), ErbB3, phosphorylated AKT1/2/3 (Ser 473), AKT 1/2/3, phosphorylated ERK (Tyr 204), ERK2, phosphorylated MEK-1/2 (Ser 218/Ser 222), MEK-1, p27, ITEM-4, NF-κB p52/p100, β-actin (all from Santa Cruz Biotechnology) and Fn14 polyclonal antibody (Cell Signaling Technology).

Combination studies of hSGZ with trastuzumab

Cells were plated into 96-well plates. After 24 h, the cells were treated with drug containing medium. At the end of the indicated incubation period, growth inhibition was assessed by crystal violet staining. IC_{25} doses of either hSGZ or 50 or 100 μg/ml trastuzumab were used in the combination studies. To determine the effects of drug sequencing, cells were treated with three different sequences: sequence I—cells were pretreated with a trastuzumab for 6 h, followed by coadministration with hSGZ for 72 h; sequence II—cells were pretreated with hSGZ for 6 h, followed by coadministration with trastuzumab for 72 h; sequence III-coexposure of hSGZ and trastuzumab to the cells for 72 h.

Pharmacokinetic study

The hSGZ was labeled with the near-infrared fluorescence dye IRDye 800CW (LI-COR Biosciences) according to the manufacturer's protocol. Female BALB/c mice (5–7 weeks old) were injected (*i.v.*, tail vein) with 80 μg of IRDye 800CW-labeled hSGZ (IR-hSGZ, ratio of Dye/Protein = 0.5). Three mice at each time point were sacrificed at 10, 20, 40, 60 minutes and 2, 4, 8, 10, 12 and 24 hours after administration. Blood samples were removed from the chest cavity and fluorescent activity assayed using IVIS 200 imaging system 200 (Xenogen Corp., filter sets: excitation/emission, 760/800 nm). The results from plasma determinations of drug concentration were analyzed by a least squares nonlinear regression using WinNonlin 5.0.1 software (Pharsight Corp., Palo Alto, CA, USA).

Biodistribution study

Fifteen Nu/Nu mice bearing MDA-MB-231/Luc tumors received intravenous injection of IRDye 800CW labeled hSGZ (Dye/Protein = 0.5) through the tail vein at a dose of 80 μg per mouse. At 24, 48 or 72 h after injection, the mice (n=5) were euthanized and dissected. Blood and organ tissues, including heart, liver, spleen, kidney, lung, stomach, intestine, uterus, skin, muscle, bone, brain and tumor, were removed from each mouse for quantitative optical imaging. The tissues were weighed, and fluorescent activity of each tissue was measured by an IVIS 100 imaging system (Xenogen Corp.) using the ICG filter sets (excitation/emission, 710–760/810–875 nm).

In vivo efficacy studies

Animal procedures were conducted according to a protocol approved by the AALAC-approved Animal Care and Use Facility at MDACC. Female BALB/c nude mice (6–8 weeks old) were injected (hind flank) subcutaneously with MDA-MB-231-LUC cells (8×10^6 cells per mouse; suspended in 100 μL of PBS mixed with 100 μL BD Matrigel). Once tumors reached a mean volume of ~100 mm^3, animals were treated (*i.v.* via tail vein) with PBS, ITEM-4 or with immunotoxins. Animals were monitored and tumors were measured every 2–3 days. Data are presented as mean tumor volume (mm^3) ± SD. Survival was calculated using a predefined cutoff volume of 1,200 mm^3 as a surrogate for mortality (30). Average percentage weight change was used as a surrogate end point for tolerability. Toxicity was defined as ≥20% of mice showing ≥20% body weight loss and/or mortality.

Bioluminescence imaging (BLI)

In vivo BLI was conducted using the IVIS100 system with Living Image acquisition and analysis software (Caliper Life Sciences). Anesthetized mice were *i.p.* injected with 75 mg/kg D-luciferin and imaged 10 min after luciferin injection.

Localization of hSGZ in tumor tissue

Twenty-four hours after *i.v.* injection of ITEM-4, ITEM4-rGel or hSGZ, the mice were sacrificed and tumor samples were collected and frozen immediately for sectioning. Localization of ITEM4-rGel and hSGZ in tumor tissues was performed as previously described (21).

Statistical analysis

Statistical analyses were conducted using GraphPad Prism with one-way ANOVA analysis, followed by Dunnet's t test to compare the tumor sizes between the control- and drug-treated groups. Survival comparisons between groups were analyzed by log-rank test (GraphPad Prism 5). Differences between groups were considered significant when the P value was ≤ 0.05.

Results

Effect of hSGZ on breast tumor cell lines

MDA-MB-231 is a triple-negative human breast cancer cell line that expresses relatively high levels of Fn14 (14). To determine whether hSGZ could specifically internalize into target cells, immunofluorescence staining was conducted on Fn14-positive and -negative cells. Confocal microsopy images showed that the rGel moiety of hSGZ was observed primarily in the cytosol of Fn14-expressing MDA-MB-231 breast cancer cells (Fig. 1A) and MDA-MB-435 melanoma cells (Supplementary Fig. 1A). We found no internalization in Fn14-deficient MEF 3.5−/− cells (data not shown).

hSGZ treatment of MDA-MB-231 cells has a comparative cytotoxicity to the parental immunoconjugate ITEM4-rGel with an IC_{50} of 0.1 nmol/L and this effect can be completely abrogated by pretreatment with the mAb ITEM-4 (Fig. 1B). Exposure to hSGZ for as short as 1 h, followed by drug removal and an additional 72-h incubation period, resulted in no significant difference in cytotoxicity compared to 72 h exposure (Fig. 1C, $p>0.05$) indicating a rapid uptake mechanism. Additional cytotoxicity assays using a panel of breast cancer cell lines, which expressed different levels of Fn14, showed that hSGZ was highly toxic to Fn14-positive cells (IC_{50} ranged from 0.1 nM-2.4 nM) and 188 to 8,350 fold more potent than free rGel. In contrast, hSGZ treatment had no significant effect on Fn14-negative BT-474 and BT-474/HR (Herceptin-resistant) breast cancer cells (Table 1) or Fn14-deficient MEF 3.5 −/− cells (Supplementary Fig. 1B). We reported previously that hSGZ-mediated cytotoxicity in melanoma cells occured via a necrotic mechanism (21). Treatment of MDA-MB-231 cells for 72 h did not induce apoptosis (Supplementary Fig. 1C). To assess whether necrotic cell death was induced in breast cancer cells, an LDH release assay was used (31). As shown in (Fig. 1D), treatment with hSGZ induced LDH release which was found to be both time- and dose-dependent and which is consistent with a necrotic cell death mechanism.

Multi-drug resistant (MDR1) tumor cells are not cross-resistant to ITEM4-rGel or hSGZ

Expression of P-glycoprotein (P-gp) encoded by the *mdr1* gene is one of the key molecules leading to resistance of cancer cells to chemotherapeutic agents (32). To evaluate the effect of MDR1 expression on immunotoxin-induced cell killing, we compared the sensitivities of MDA-MB-435/LCC6^{MDR1}and HeyA8-MDR cells and their parental counterparts (MDA-

MB-435 and HeyA8) to Fn14-targeted immunotoxins. We also tested the activity of two other cytotoxic compounds-paclitaxel and doxrubicin -which have previously been shown to be MDR1 substrates (32, 33). As expected, paclitaxel and doxorubicin were less potent in killing the P-gp–overexpressing human melanoma MDA-MB-435/LCC6^{MDR1} cells and the paclitaxel-derived ovarian cancer HeyA8-MDR cells than in killing their corresponding parental cells (Table 2). These results indicate that MDR1 activity limits the potency of these conventional cytotoxic compounds. In contrast, the IC_{50}s of ITEM4-rGel and hSGZ on the MDR cells were similar to their parental cells (less than ~ 1-fold for both MDR cell lines, respectively; Table 2), suggesting that rGel-based immunotoxins may be effective in overcoming MDR1-mediated multidrug resistance in cancer.

hSGZ inhibits Erb3/Akt signaling in HER2-overexpressing breast cancer cells

Fn14 and HER2 are frequently co-expressed in human breast tumors (14, 23) and HER2 signaling in breast cancer cells directly induces Fn14 gene (34). To determine if HER2-induced up-regulation of Fn14 expression would sensitize cells to hSGZ treatment, MCF7 and MCF7/HER2 cells were exposed to hSGZ. Increased Fn14 protein expression by HER2 overexpression was confirmed by flow cytometry (Fig. 2A). MCF7/HER2 cells were more sensitive to hSGZ treatment with a 3.4-fold decreased IC_{50} dose compared to MCF7 cells (Fig. 2B). This finding suggests that induced overexpression of Fn14 by HER2 signaling could be translated to an improved therapeutic index with immunotoxin treatment.

The two most prevalent downstream signaling pathways activated in HER2-overexpressing breast cancer cells are the Ras/MAPK and the phosphatidylinositol 3-kinase (PI3K)/AKT pathways. To further understand the mechanism of action and potency of hSGZ on HER2+ breast cancer cells, we explored the HER2 signaling pathway in MCF7 and MCF7/HER2 cells in the absence or presence of hSGZ. As shown in Fig. 2C, HER2 overexpression induced robust phosphorylation of HER2, HER3 (ErbB3) and Akt in MCF7 cells as assessed by Western blot. In MCF7/HER2 cells, hSGZ significantly suppressed HER3 and Akt phosphorylation in a dose-dependent manner without effecting HER2 phosphorylation (Fig. 2C). hSGZ treatment also decreased the total level of HER3 in MCF7 cells but not in MCF7/HER2 cells. Overexpression of HER2 in MCF7 cells increased Fn14 expression as expected (34); however, treatment with hSGZ also dose-dependently increased Fn14 levels (Fig. 2C), which is consistent with our previous report demonstrating that hSGZ can up-regulate Fn14 expression (21). hSGZ treatment dose-dependently suppressed Erk2 and phospho-Erk1/2 levels (Fig. 2D). Treatment also increased both NF-kB p52 and NF-kB p100 levels in both cell lines and decreased p27 levels (Fig. 2D). This latter effect is probably due to a decrease in regulatory, rapid-turnover proteins as a result of the overall inhibition of protein synthesis by the rGel component of the immunotoxin. These results indicate that the Fn14 receptor may be an important downstream regulator of HER2/HER3 signaling in breast cancer cells and that hSGZ treatment can suppress HER3/Akt activation in HER2-overexpressing cells.

hSGZ in combination with trastuzumab shows additive/synergistic effects on HER2+/Fn14+ breast cancer cells

We next examined the effects of hSGZ in combination with trastuzumab, which is currently used to treat patients with HER2-overexpressing breast cancer (35, 36), on MCF7 and MCF7/HER2 cells. As expected, treatment of HER2-negative MCF7 cells with 50 or 100 μg/ml of trastuzumab (T) had little effect on cell viability and co-treatment with an IC_{25} dose of hSGZ produced a cytotoxic effect similar to hSGZ alone (Fig. 3A). In contrast, although 50 or 100 μg/ml of trastuzumab has marginal growth inhibition effect on MCF7/HER2 cells, IC_{25} dose of hSGZ when combined with 50 or 100 μg/ml of trastuzumab treatment markedly increased its cytotoxic effect to ~ 50% of viability (Fig. 3A). hSGZ also potentiated trastuzumab's cytotoxic effect on SKBR3 breast cancer cells, which have high

endogenous expression levels of both the HER2 and Fn14 receptors (Fig. 3B). The data (Fig. 3B) suggest that simultaneous addition of hSGZ and trastuzumab (T) was significantly ($p < 0.05$) more active than either addition of hSGZ followed by T, or T followed by hSGZ.

Pharmacokinetics of hSGZ

Pharmacokinetic data was obtained using hSGZ labeled with the near infrared (NIR) dye 800CW (IR-hSGZ, Supplementary Fig. 3A) after intravenous administration in mice. As shown in Fig. 4A, there was a bi-exponential disposition of IR-hSGZ in the blood. Following intravenous administration, IR-hSGZ had a rapid initial distribution to a highly perfused, central compartment (mean $t_{1/2\,\alpha} = 1.26$ h), followed by an extensive distribution to a second tissue compartment (mean $t_{1/2\,\beta} = 7.29$ h), during which the fluorescent-conjugate spread from the central blood compartment to the extravascular space of the solid tissues. The initial concentration of IR-hSGZ in the plasma was 24.9 ± 2.9 μg/mL, which corresponded to the injected dose of the drug. The pharmacokinetic parameters are summarized in Fig. 4A (right).

Biodistribution of hSGZ

NIR images were taken at 24, 48 and 72 h postinjection of fluorescent labeled hSGZ into nude mice bearing MDA-MB-231/Luc tumors and showed an accumulation of fluorescence in the organs and tumors (Fig. 4B and Supplementary Fig. 3B). BLI imaging of the MDA-MB-231/Luc primary tumors corresponding to the NIR images of the same mice clearly showed the IR-hSGZ was colocalized in the tumor tissues (Fig. 4B). To avoid any measuring errors caused by limited tissue penetration of fluorophores, animals were sacrificed, tumor and major organs were collected at the 24, 48 and 72 h time points, and then subjected immediately to NIR imaging (Supplementary Fig. 3C). The %ID/g tissue of IR-hSGZ in organs and tissues dissected at different times after fluorescent tracer injection is summarized in Fig. 4C. The liver showed the highest uptake among the tissues studied (32.5 ± 3.9 %; 27.7 ± 16.1 % and 9.2 ± 1.9 % for 24, 48 and 72 h, respectively). All the tissues except the tumors showed decreased drug uptake over time. However, the tumors showed the middle level of uptake among the tissues but with a steady pattern over time (5.1 ± 0.5 %; 4.8 ± 1.1 % and 4.7 ± 1.4 % for 24, 48 and 72 h, respectively). Similar biodistribution patterns were observed when the data was plotted as a tissue-to-muscle ratio (Supplementary Fig. 3D). IR-hSGZ accumulation in the tumor was further indicated by the increasing tumor-to-muscle ratio post-IR-hSGZ injection over time (Supplementary Fig. 3D) (5.6 ± 1.3; 6.2 ± 1.6 and 9.0 ± 2.3 for 24, 48 and 72 h, respectively).

Efficacy of hSGZ in breast cancer xenograft model

We next examined the effect of hSGZ on the growth of established tumors using a MDA-MB-231/Luc xenograft model of human breast cancer. Primary tumor sizes were assessed by either caliper measurement or BLI imaging. A significant tumor growth inhibition was observed at both doses of the hSGZ (25 or 36 mg/kg) compare to saline control ($P < 0.01$) (Fig. 5A). The tumors remained static for the entire study period of more than 40 days in response to dose of 36 mg/kg for ITEM4-rGel ($P = 0.009$) (Fig. 5A). Mice treated with 36 mg/kg ITEM-4 plus rGel also had marginal tumor growth relative to the saline control, but there was no significant difference between these two groups ($P = 0.06$, on day 28). Survival in the mice treated with ITEM4-rGel and hSGZ was significantly better than in those treated with saline or with ITEM-4 plus rGel ($P < 0.0001$) (Fig. 5B). Compared with animals in the saline group, ITEM-4 plus rGel treated mice showed a 48% increased life span. The representative BLI images of the tumors on selected days clearly demonstrated the antitumor properties of the ITEM4-rGel and hSGZ (Fig. 5C). Since the ITEM-4 antibody can recognize murine Fn14, we were also able to assess immunotoxin toxicity against normal mouse tissues. Toxicity was monitored by frequent body weight measurements. The mouse

body weights showed less than a 20% change in any of the treated or control groups over the duration of the experiment (Fig. 5D). We also found Fn14 was up-regulated after treatment with anti-Fn14 antibody ITEM-4 and ITEM4-based immunotoxins (ITEM4-rGel and hSGZ) *in vivo* as assayed by Western blot analysis of tumor tissues (Fig. 5E). Immunofluorescence staining confirmed that ITEM4-rGel and hSGZ localized specifically in tumor tissue and no nonspecific staining was observed in tumors after administration of ITEM-4 plus rGel and saline detected by anti-rGel antibody (Supplementary Fig. 4).

Discussion

Three separate groups have now independently reported that Fn14 is frequently overexpressed in breast tumors compared to normal breast epithelium (11, 14, 22, 23). Overexpression of Fn14 was found to be positively correlated with metastasis, positive lymph nodes and $HER2^{+}/ER^{-}$ status, which are three indicators of poor prognosis of breast cancer patients (14, 23). Our group recently demonstrated that Fn14 is overexpressed in 173/190 (92%) of melanoma biopsy specimens tested (21) suggesting that an anti-Fn14 approach could also be useful for this tumor type. The differential expression of Fn14 in HER2+ breast tumors compared to normal tissue prompted us to test the Fn14-targeted immunotoxin hSGZ as an alternative anti-tumor strategy beyond the currently used HER2-directed therapeutics trastuzumab and lapatinib. Because the cytotoxic mechanism of hSGZ is markedly distinct from these two agents, it is a potential alternative for HER2+ breast cancer patients resistant to current therapeutic approaches.

The development of resistance to chemotherapeutic agents through emergence of tumor cells expressing a multidrug-resistant (MDR) phenotype (33) is a well-known and well-characterized event. The P-glycoprotein transporter (MDR1)-mediated efflux of anticancer drugs is the most commonly observed MDR phenotype clinically, and correlations between the transporter expression and poor response to chemotherapy have been documented for many cancer types (32, 37). The results of the cytotoxicity studies indicate that the ITEM4-rGel and hSGZ constructs display similar sensitivity to MDR-1-overexpressing tumor cell lines (Table 2), supporting the possibility that rGel-based immunotoxins may be effective in targeting solid tumors resistant to conventional agents.

The HER family (ErbB1/EGFR, ErbB2/HER2, ErbB3, and ErbB4) of transmembrane proteins has been firmly established as important drivers and therapeutic targets in solid tumors (38, 39). Recently, Whitsett *et al.* (40) reported that high Fn14 levels correlated with EGFR (HER1) activation in non-small cell lung cancer specimens and cell lines. In addition, the Fn14 and HER2 receptors are frequently coexpressed in breast tumors (14, 23), and Fn14 is a HER2-inducible gene (34). We report here that the increased Fn14 expression by HER2 signaling in MCF-7 cells could be translated to better therapeutic index by targeting Fn14 when using hSGZ (Fig. 2B). The correlation of Fn14 and ErbB family member activation suggests that therapeutic targeting of Fn14 in tumors driven by oncogenic ErbB family members could benefit patients.

HER2/ErbB3 heterodimers have been found to be powerful oncogene drivers, in part, because ErbB3 activation amplifies signaling through phosphatidyl inositol 3-kinase (PI3K) (41). It is thought that ErbB3 functions primarily to drive HER2-mediated PI3K signaling (42, 43). ErbB3 promotes HER2-induced changes in the breast epithelium before, during, and after tumor formation (44). Recent studies suggest that HER2-amplified breast cancer cells employ HER3/ErbB3 to promote therapeutic resistance to HER2 inhibitors trastuzumab and the dual EGFR/ErbB2 TK inhibitor lapatinib (45).

Because ErbB2 inhibitors initially cause a decrease in P-ErbB3/PI3K signaling (46–48), many metastatic HER2-amplified breast cancers do not respond or eventually escape trastuzumab- and lapatinib-mediated growth inhibition, often with recovery of ErbB3/PI3K signaling (45). Thus, the HER3-PI3K node is emerging as a potential target for anticancer therapy (49, 50). Our study demonstrates that targeting Fn14 by hSGZ inhibits ErbB3/Akt signaling in HER2 over-expressing MCF-7 breast cancer cells (Fig. 2C). These results suggest that hSGZ has the potential to overcome trastuzumab or lapatinib resistance in HER2+ breast tumors.

Clinical trials using pertuzumab and trastuzumab in combination in advanced HER2+ breast cancers have demonstrated significant clinical activity (51). Thus, there is a rationale for combining HER2-targeted agents with Fn14-targeted agents such as hSGZ. Our studies on MCF7-HER2 cells clearly demonstrate that treatment with hSGZ augments the therapeutic efficacy of trastuzumab (Fig. 3). Furthermore, *in vitro* combination studies on MDA-MB-435 melanoma cells using hSGZ and several standard chemotherapeutic agents also showed a synergistic and/or additive cytotoxic effect (Supplementary Fig. 2). These data suggest that consideration should be given to eventual clinical trials with combinations of hSGZ and trastuzumab or standard chemotherapeutic agents.

The pharmacokinetic data for IR-hSGZ were best characterized by biexponential kinetics with a rapid initial clearance phase followed by a more prolonged clearance phase after intravenous administration (Fig. 4A). The prolonged disposition of IR-hSGZ in mice is likely attributable to the relatively large size of the dimerized fusion protein (120 kDa). The prolonged circulation of IR-hSGZ in blood allows for accumulation and retention of the fusion protein in the tumor over time, as shown in the NIR and BLI imaging study in mice bearing MDA-MB-231/Luc tumors (Fig. 4B and Supplementary Fig. 3). The tumor/muscle ratio of hSGZ was shown to increase over time and reached the highest level at 72 h post-injection of the IR-hSGZ (Fig. 4C and Supplementary Fig. 3D) which suggested that hSGZ was efficiently delivered to the tumor site.

The biodistribution data obtained in our study should be useful for determining dosing schedules, establishing efficacy, and predicting possible toxicity. As expected, the highest levels of drug were found in highly perfused organs such as liver, kidneys and spleen (Fig. 4C). Retention in the liver may also suggest that the liver may be involved in hSGZ metabolism and but no overt toxicity was observed in mice even at the highest doses employed. It is important to note that the anti-Fn14 antibody employed for hSGZ construction cross-reacts with murine Fn14 receptors. Therefore, any toxicity observed is likely to be more relevant to eventual clinical studies.

Our preclinical antitumor studies using a five day interval treatment schedule based on pharmacokinetic and imaging data showed therapeutic efficacy of hSGZ in MDA-MB-231/Luc tumors (Fig. 5). Consistent with our previous melanoma studies, we showed that ITEM4-rGel was more potent than hSGZ in this breast cancer xenograft model. However, hSGZ showed reduced systemic toxicity compared to ITEM4-rGel as assessed by body weight measurements (Fig. 5D). Fn14 expression was up-regulated by treatment with hSGZ *in vitro* (Fig. 2C) and *in vivo* (Fig.5E), which was consistent with our previous results (21).

Recently, we reported Phase 1 clinical studies of an rGel immunoconjugate containing the anti-CD33 antibody HuM195. These studies demonstrated limited antigenicity and no vascular leak issues with rGel-based therapeutics even after repeated administration (52). These promising preclinical activities of hSGZ will need to be confirmed by clinical trials. Overall, our data suggest that hSGZ is a potent anticancer agent with a novel mechanism of

action that might prove to be effective against multiple Fn14-positive tumor types resistant to conventional agents.

Supplementary Material

Refer to Web version on PubMed Central for supplementary material.

Acknowledgments

We thank Dr. Dihua Yu (MD Anderson Cancer Center) for providing the MCF7/HER2 cell line and Dr. Robert Clarke (Georgetown University, Washington, DC) for the MDA-MB-435/LCC6 ^{MDR1} cells. We also wish to thank Dr. Dong Liang (College of Pharmacy, Texas Southern University, Houston, TX) for analyzing the pharmacokinetic data.

Funding:

This work was supported, in part, by the Clayton Foundation for Research (MGR), Susan G. Komen Foundation grant KG100240 (SSM), National Institutes of Health grant R01 NS055126 (JAW), and Department of Defense Breast Cancer Concept Award BC086135 (JAW).

Abbreviation list

TNF	Tumor necrosis factor
TWEAK	TNF-like weak inducer of apoptosis
Fn14	fibroblast growth factor-inducible protein 14
rGel	recombinant gelonin

Reference List

1. Jemal A, Bray F, Center MM, Ferlay J, Ward E, Forman D. Global cancer statistics. CA Cancer J Clin. 2011; 61:69–90. [PubMed: 21296855]
2. Tsang RY, Finn RS. Beyond trastuzumab: novel therapeutic strategies in HER2-positive metastatic breast cancer. Br J Cancer. 2012; 106:6–13. [PubMed: 22215104]
3. Gucalp A, Traina TA. Triple-negative breast cancer: adjuvant therapeutic options. Chemother Res Pract. 2011; 2011:696208. [PubMed: 22312556]
4. Wiley SR, Cassiano L, Lofton T, Davis-Smith T, Winkles JA, Lindner V, et al. A novel TNF receptor family member binds TWEAK and is implicated in angiogenesis. Immunity. 2001; 15:837–846. [PubMed: 11728344]
5. Burkly LC, Michaelson JS, Hahm K, Jakubowski A, Zheng TS. TWEAKing tissue remodeling by a multifunctional cytokine: role of TWEAK/Fn14 pathway in health and disease. Cytokine. 2007; 40:1–16. [PubMed: 17981048]
6. Winkles JA. The TWEAK-Fn14 cytokine-receptor axis: discovery, biology and therapeutic targeting. Nat Rev Drug Discov. 2008; 7:411–425. [PubMed: 18404150]
7. Michaelson JS, Burkly LC. Therapeutic targeting of TWEAK/Fnl4 in cancer: exploiting the intrinsic tumor cell killing capacity of the pathway. Results Probl Cell Differ. 2009; 49:145–160. [PubMed: 19513634]
8. Maecker H, Varfolomeev E, Kischkel F, Lawrence D, LeBlanc H, Lee W, et al. TWEAK attenuates the transition from innate to adaptive immunity. Cell. 2005; 123:931–944. [PubMed: 16325585]
9. Kaduka Y, Takeda K, Nakayama M, Kinoshita K, Yagita H, Okumura K. TWEAK mediates anti-tumor effect of tumor-infiltrating macrophage. Biochem Biophys Res Commun. 2005; 331:384–390. [PubMed: 15850771]
10. Michaelson JS, Amatucci A, Kelly R, Su L, Garber E, Day ES, et al. Development of an Fn14 agonistic antibody as an anti-tumor agent. MAbs. 2011; 3:362–375. [PubMed: 21697654]

11. Culp PA, Choi D, Zhang Y, Yin J, Seto P, Ybarra SE, et al. Antibodies to TWEAK receptor inhibit human tumor growth through dual mechanisms. Clin Cancer Res. 2010; 16:497–508. [PubMed: 20068083]
12. Tran NL, McDonough WS, Donohue PJ, Winkles JA, Berens TJ, Ross KR, et al. The human Fn14 receptor gene is up-regulated in migrating glioma cells in vitro and overexpressed in advanced glial tumors. Am J Pathol. 2003; 162:1313–1321. [PubMed: 12651623]
13. Tran NL, McDonough WS, Savitch BA, Fortin SP, Winkles JA, Symons M, et al. Increased fibroblast growth factor-inducible 14 expression levels promote glioma cell invasion via Rac1 and nuclear factor-kappaB and correlate with poor patient outcome. Cancer Res. 2006; 66:9535–9542. [PubMed: 17018610]
14. Willis AL, Tran NL, Chatigny JM, Charlton N, Vu H, Brown SA, et al. The fibroblast growth factor-inducible 14 receptor is highly expressed in HER2-positive breast tumors and regulates breast cancer cell invasive capacity. Mol Cancer Res. 2008; 6:725–734. [PubMed: 18505918]
15. Watts GS, Tran NL, Berens ME, Bhattacharyya AK, Nelson MA, Montgomery EA, et al. Identification of Fn14/TWEAK receptor as a potential therapeutic target in esophageal adenocarcinoma. Int J Cancer. 2007; 121:2132–2139. [PubMed: 17594693]
16. Wang S, Zhan M, Yin J, Abraham JM, Mori Y, Sato F, et al. Transcriptional profiling suggests that Barrett's metaplasia is an early intermediate stage in esophageal adenocarcinogenesis. Oncogene. 2006; 25:3346–3356. [PubMed: 16449976]
17. Huang M, Narita S, Tsuchiya N, Ma Z, Numakura K, Obara T, et al. Overexpression of Fn14 promotes androgen-independent prostate cancer progression through MMP-9 and correlates with poor treatment outcome. Carcinogenesis. 2011; 32:1589–1596. [PubMed: 21828059]
18. Kwon OH, Park SJ, Kang TW, Kim M, Kim JH, Noh SM, et al. Elevated fibroblast growth factor-inducible 14 expression promotes gastric cancer growth via nuclear factor-kappaB and is associated with poor patient outcome. Cancer Lett. 2012; 314:73–81. [PubMed: 21993017]
19. Als AB, Dyrskjot L, von der MH, Koed K, Mansilla F, Toldbod HE, et al. Emmprin and survivin predict response and survival following cisplatin-containing chemotherapy in patients with advanced bladder cancer. Clin Cancer Res. 2007; 13:4407–4414. [PubMed: 17671123]
20. Wang S, Jiang W, Chen X, Zhang C, Li H, Hou W, et al. Alpha-fetoprotein acts as a novel signal molecule and mediates transcription of Fn14 in human hepatocellular carcinoma. J Hepatol. 2012; 57:322–329. [PubMed: 22521346]
21. Zhou H, Ekmekcioglu S, Marks JW, Mohamedali KA, Asrani K, Phillips KK, et al. The TWEAK receptor Fn14 is a therapeutic target in melanoma: Immunotoxins targeting Fn14 receptor for malignant melanoma treatment. J Invest Dermatol. 2013; 133:1052–1062. [PubMed: 23190886]
22. Michaelson JS, Cho S, Browning B, Zheng TS, Lincecum JM, Wang MZ, et al. Tweak induces mammary epithelial branching morphogenesis. Oncogene. 2005; 24:2613–2624. [PubMed: 15735761]
23. Chao DT, Su M, Tanlimco S, Sho M, Choi D, Fox M, et al. Expression of TweakR in breast cancer and preclinical activity of enavatuzumab, a humanized anti-TweakR mAb. J Cancer Res Clin Oncol. 2013; 139:315–325. [PubMed: 23073510]
24. Michaelson JS, Kelly R, Yang L, Zhang X, Wortham K, Joseph IB. The anti-Fn14 antibody BIIB036 inhibits tumor growth in xenografts and patient derived primary tumor models and enhances efficacy of chemotherapeutic agents in multiple xenograft models. Cancer Biol Ther. 2012; 13:812–821. [PubMed: 22669574]
25. Zhou H, Marks JW, Hittelman WN, Yagita H, Cheung LH, Rosenblum MG, et al. Development and characterization of a potent immunoconjugate targeting the Fn14 receptor on solid tumor cells. Mol Cancer Ther. 2011; 10:1276–1288. [PubMed: 21586630]
26. Balzer EM, Whipple RA, Thompson K, Boggs AE, Slovic J, Cho EH, et al. c-Src differentially regulates the functions of microtentacles and invadopodia. Oncogene. 2010; 29:6402–6408. [PubMed: 20956943]
27. Leonessa F, Green D, Licht T, Wright A, Wingate-Legette K, Lippman J, et al. MDA435/LCC6 and MDA435/LCC6MDR1: ascites models of human breast cancer. Br J Cancer. 1996; 73:154–161. [PubMed: 8546900]

28. Apte SM, Fan D, Killion JJ, Fidler IJ. Targeting the platelet-derived growth factor receptor in antivascular therapy for human ovarian carcinoma. Clin Cancer Res. 2004; 10:897–908. [PubMed: 14871965]
29. Nakayama M, Ishidoh K, Kojima Y, Harada N, Kominami E, Okumura K, et al. Fibroblast growth factor-inducible 14 mediates multiple pathways of TWEAK-induced cell death. J Immunol. 2003; 170:341–348. [PubMed: 12496418]
30. Yang H, Higgins B, Kolinsky K, Packman K, Go Z, Iyer R, et al. RG7204 (PLX4032), a selective BRAFV600E inhibitor, displays potent antitumor activity in preclinical melanoma models. Cancer Res. 2010; 70:5518–5527. [PubMed: 20551065]
31. Do TN, Rosal RV, Drew L, Raffo AJ, Michl J, Pincus MR, et al. Preferential induction of necrosis in human breast cancer cells by a p53 peptide derived from the MDM2 binding site. Oncogene. 2003; 22:1431–1444. [PubMed: 12629507]
32. Leonard GD, Fojo T, Bates SE. The role of ABC transporters in clinical practice. Oncologist. 2003; 8:411–424. [PubMed: 14530494]
33. Szakacs G, Paterson JK, Ludwig JA, Booth-Genthe C, Gottesman MM. Targeting multidrug resistance in cancer. Nat Rev Drug Discov. 2006; 5:219–234. [PubMed: 16518375]
34. Asrani K, Keri RA, Galisteo R, Brown SA, Morgan SJ, Ghosh A, et al. The HER2- and heregulin β1 (HRG)-inducible TNFR superfamily member Fn14 promotes HRG-driven cell migration, invasion and MMP9 expression. Mol Cancer Res. 2013 epub ahead of print.
35. Cobleigh MA, Vogel CL, Tripathy D, Robert NJ, Scholl S, Fehrenbacher L, et al. Multinational study of the efficacy and safety of humanized anti-HER2 monoclonal antibody in women who have HER2-overexpressing metastatic breast cancer that has progressed after chemotherapy for metastatic disease. J Clin Oncol. 1999; 17:2639–2648. [PubMed: 10561337]
36. Vogel CL, Cobleigh MA, Tripathy D, Gutheil JC, Harris LN, Fehrenbacher L, et al. Efficacy and safety of trastuzumab as a single agent in first-line treatment of HER2-overexpressing metastatic breast cancer. J Clin Oncol. 2002; 20:719–726. [PubMed: 11821453]
37. Takara K, Sakaeda T, Okumura K. An update on overcoming MDR1-mediated multidrug resistance in cancer chemotherapy. Curr Pharm Des. 2006; 12:273–286. [PubMed: 16454744]
38. Yarden Y, Sliwkowski MX. Untangling the ErbB signalling network. Nat Rev Mol Cell Biol. 2001; 2:127–1237. [PubMed: 11252954]
39. Hynes NE, Macdonald G. ErbB receptors and signaling pathways in cancer. Curr Opin Cell Biol. 2009; 21:177–184. [PubMed: 19208461]
40. Whitsett TG, Cheng E, Inge L, Asrani K, Jameson NM, Hostetter G, et al. Elevated expression of Fn14 in non-small cell lung cancer correlates with activated EGFR and promotes tumor cell migration and invasion. Am J Pathol. 2012; 181:111–120. [PubMed: 22634180]
41. Holbro T, Beerli RR, Maurer F, Koziczak M, Barbas CF III, Hynes NE. The ErbB2/ErbB3 heterodimer functions as an oncogenic unit: ErbB2 requires ErbB3 to drive breast tumor cell proliferation. Proc Natl Acad Sci U S A. 2003; 100:8933–8938. [PubMed: 12853564]
42. Chakrabarty A, Rexer BN, Wang SE, Cook RS, Engelman JA, Arteaga CL. H1047R phosphatidylinositol 3-kinase mutant enhances HER2-mediated transformation by heregulin production and activation of HER3. Oncogene. 2010; 29:5193–5203. [PubMed: 20581867]
43. Lee-Hoeflich ST, Crocker L, Yao E, Pham T, Munroe X, Hoeflich KP, et al. A central role for HER3 in HER2-amplified breast cancer: implications for targeted therapy. Cancer Res. 2008; 68:5878–5887. [PubMed: 18632642]
44. Vaught DB, Stanford JC, Young C, Hicks DJ, Wheeler F, Rinehart C, et al. HER3 Is Required for HER2-Induced Preneoplastic Changes to the Breast Epithelium and Tumor Formation. Cancer Res. 2012; 72:2672–2682. [PubMed: 22461506]
45. Garrett JT, Arteaga CL. Resistance to HER2-directed antibodies and tyrosine kinase inhibitors: mechanisms and clinical implications. Cancer Biol Ther. 2011; 11:793–800. [PubMed: 21307659]
46. Garrett JT, Olivares MG, Rinehart C, Granja-Ingram ND, Sanchez V, Chakrabarty A, et al. Transcriptional and posttranslational up-regulation of HER3 (ErbB3) compensates for inhibition of the HER2 tyrosine kinase. Proc Natl Acad Sci U S A. 2011; 108:5021–5026. [PubMed: 21385943]

47. Rexer BN, Engelman JA, Arteaga CL. Overcoming resistance to tyrosine kinase inhibitors: lessons learned from cancer cells treated with EGFR antagonists. Cell Cycle. 2009; 8:18–22. [PubMed: 19106609]

48. Abramson V, Arteaga CL. New strategies in HER2-overexpressing breast cancer: many combinations of targeted drugs available. Clin Cancer Res. 2011; 17:952–958. [PubMed: 21248299]

49. Schoeberl B, Faber AC, Li D, Liang MC, Crosby K, Onsum M, et al. An ErbB3 antibody, MM-121, is active in cancers with ligand-dependent activation. Cancer Res. 2010; 70:2485–2494. [PubMed: 20215504]

50. Schaefer G, Haber L, Crocker LM, Shia S, Shao L, Dowbenko D, et al. A two-in-one antibody against HER3 and EGFR has superior inhibitory activity compared with monospecific antibodies. Cancer Cell. 2011; 20:472–486. [PubMed: 22014573]

51. Baselga J, Cortes J, Kim SB, Im SA, Hegg R, Im YH, et al. Pertuzumab plus trastuzumab plus docetaxel for metastatic breast cancer. N Engl J Med. 2012; 366:109–119. [PubMed: 22149875]

52. Borthakur G, Rosenblum MG, Talpaz M, Daver N, Ravandi F, Faderl S, et al. Phase 1 study of an anti-CD33 immunotoxin, humanized monoclonal antibody M195 conjugated to recombinant gelonin (HUM-195/rGEL), in patients with advanced myeloid malignancies. Haematologica. 2013; 98:217–221. [PubMed: 22875630]

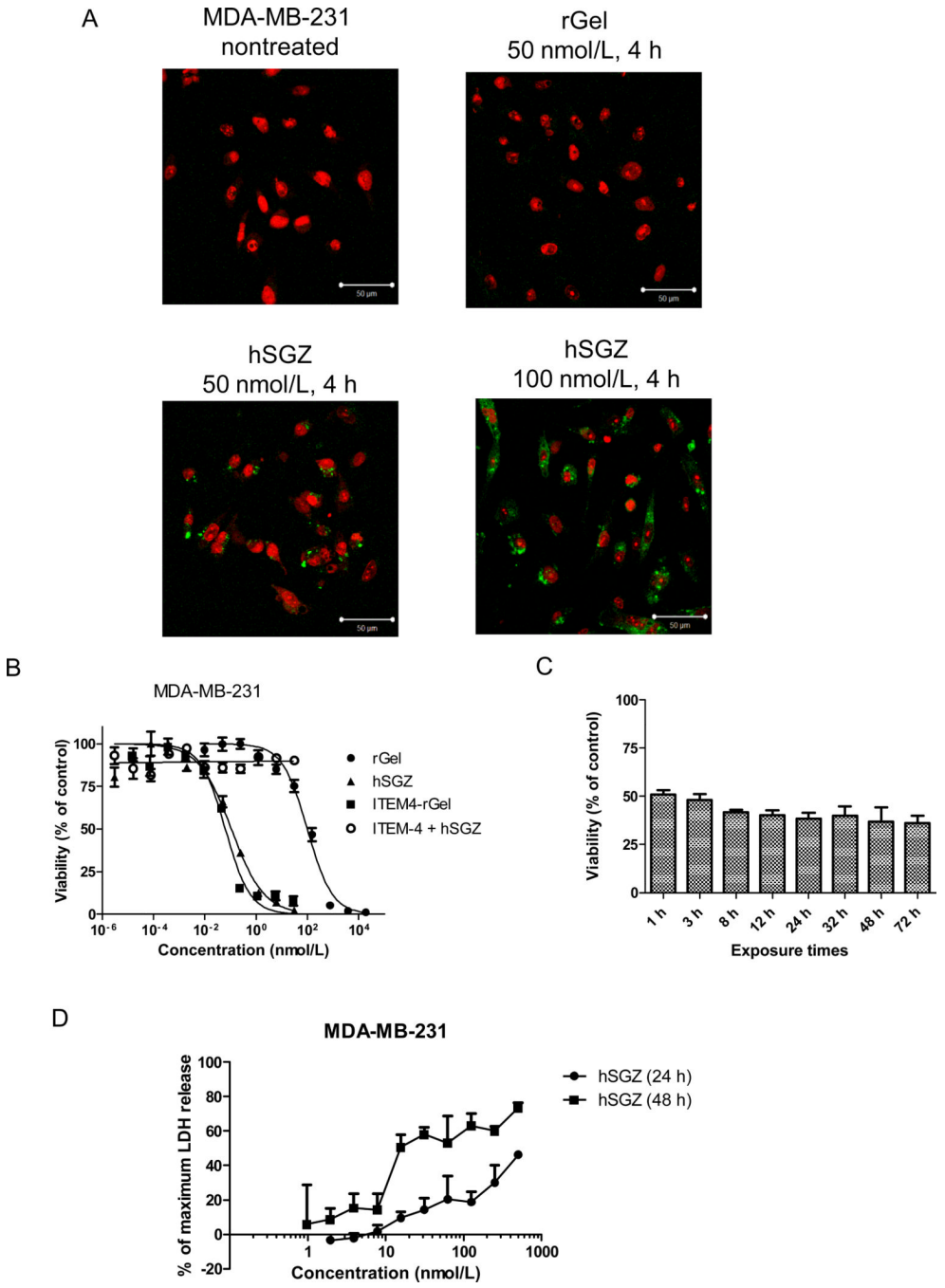

Figure 1.

Effect of the humanized, dimeric single-chain immunotoxin hSGZ on MDA-MB-231 cells. **A**, cells with either left untreated or treated with 50 nmol/L rGel and 50 or 100 nmol/L hSGZ for 4 h. The cells were fixed, acid washed to remove surface-bound material, permeabilized, and immunostained for the presence of rGel (green). The cells were counterstained with propidium iodide (red) to identify nuclei and visualized using a confocal microscope. Bar=50 μm. **B**, cells were treated with indicated concentration of rGel, ITEM4-rGel or hSGZ for 72 h. Additionally, cells were pretreated with 1 μmol/L ITEM-4 for 2 h and then coincubated with different concentration of hSGZ for another 72 h. Cell viability

was assessed by crystal violet staining. **C**, cells were plated and then exposed to hSGZ at 0.3 nmol/L for indicated periods of time. Cell viability was assessed at 72 h as described above. **D**, cells were treated with different concentrations of hSGZ for 24 or 48 h and LDH release was measured. Treatment of cells with Triton X-100 served as a positive control causing maximum LDH release. Results represent mean ± SD, n = 3.

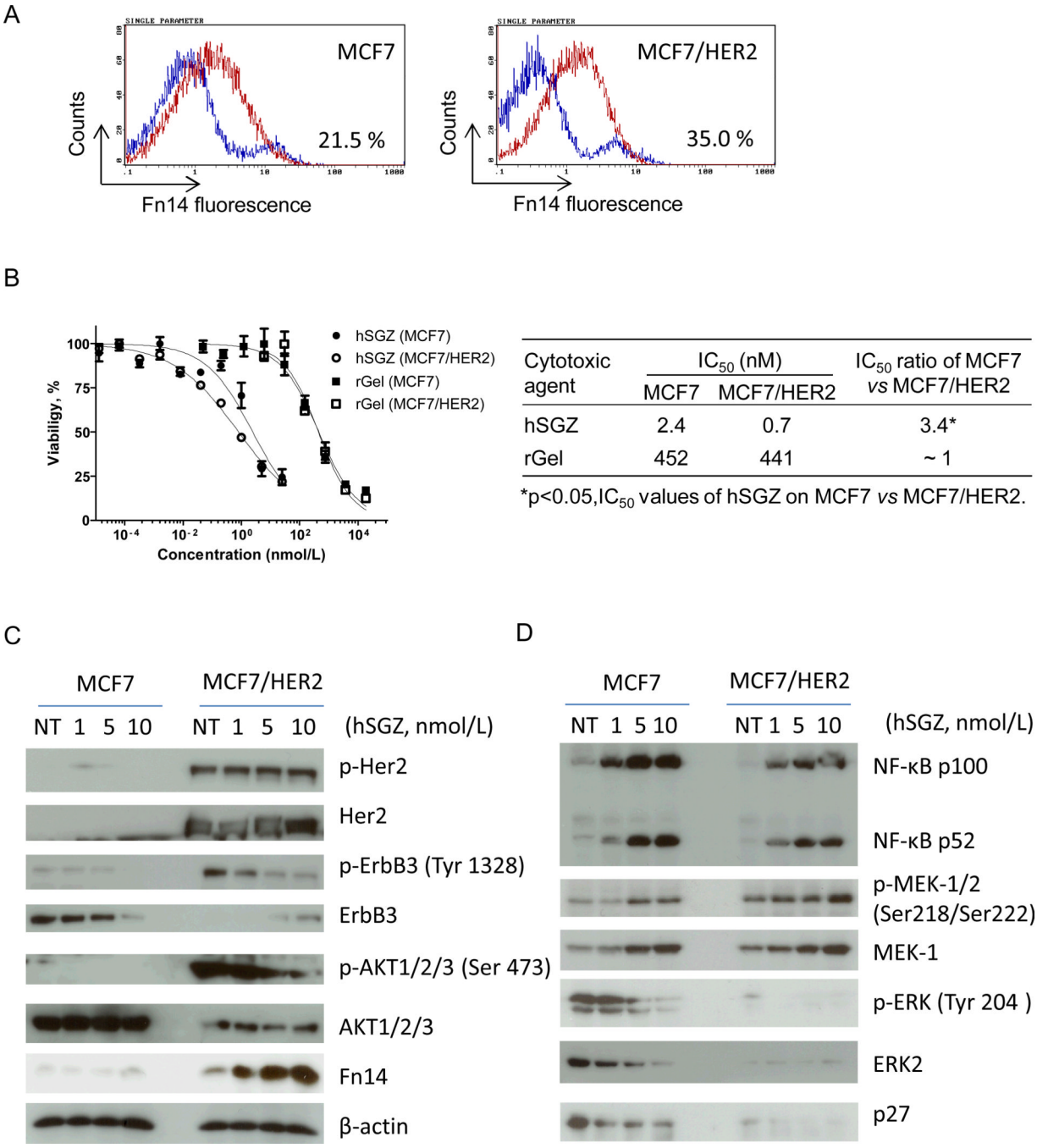

Cytotoxic agent	IC_{50} (nM)		IC_{50} ratio of MCF7 *vs* MCF7/HER2
	MCF7	MCF7/HER2	
hSGZ	2.4	0.7	3.4*
rGel	452	441	~ 1

*$p<0.05$, IC_{50} values of hSGZ on MCF7 *vs* MCF7/HER2.

Figure 2.

Effect of hSGZ treatment on MCF-7 and MCF-7/HER2 cells. **A**, parental MCF-7 cells and MCF-7 cells that stably overexpress HER2 (MCF-7/HER2) were analyzed for Fn14 cell surface expression by flow cytometry. **B**, cytotoxic effects of rGel, ITEM4-rGel and hSGZ were analyzed on MCF-7 and MCF-7/HER2 cells. Student's t test was used to calculate statistical significance. Data are representative of three independent experiments. **C** and **D**, MCF-7 and MCF-7/HER2 cells were treated with indicated concentration of hSGZ for 48 h and whole cell lysates were analyzed by Western blot with the indicated antibodies.

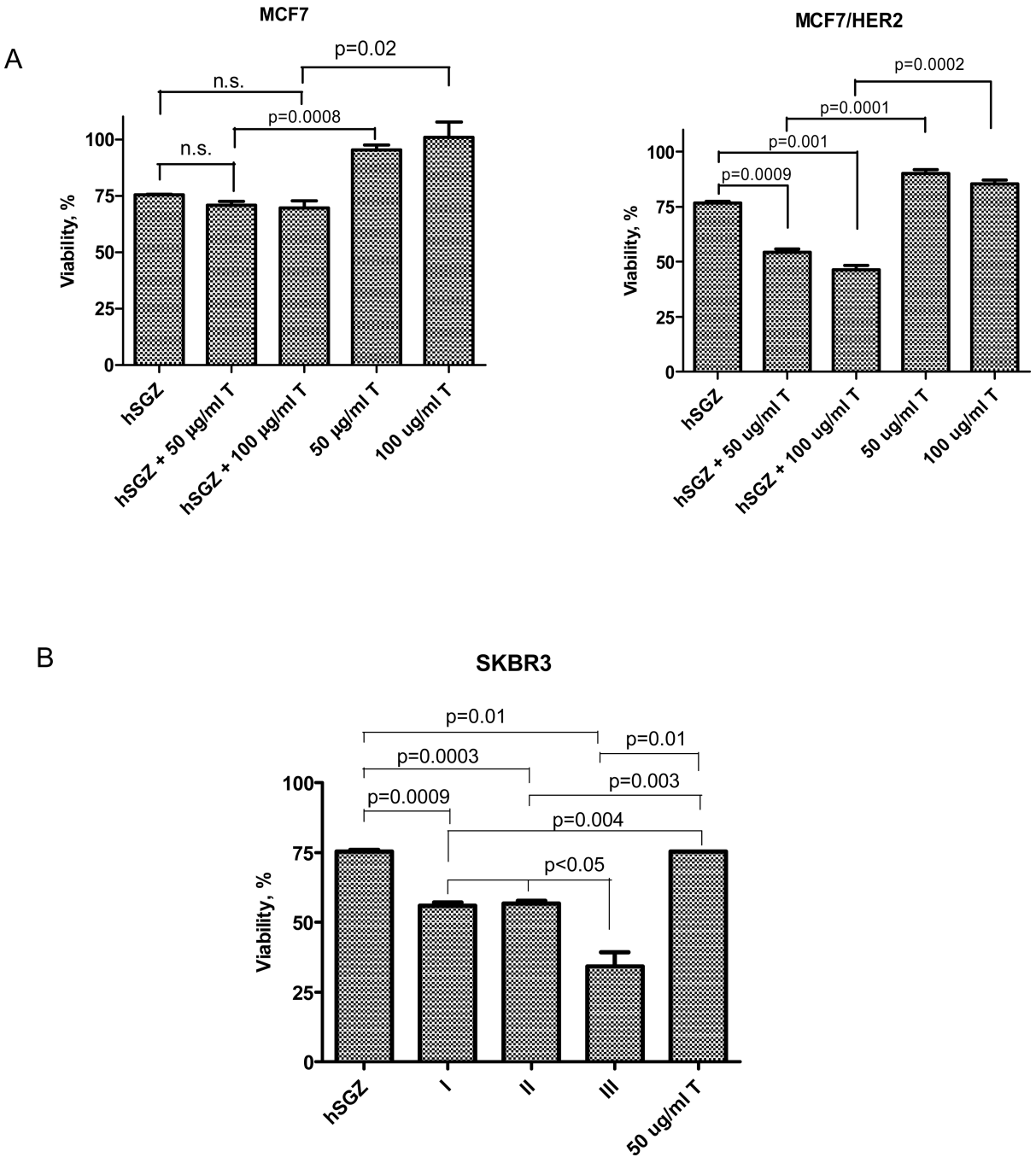

Figure 3.

Effect of hSGZ in combination with trastuzumab (T) in breast cancer cell lines. **A**, MCF-7 and MCF-7/HER2 cells were treated with hSGZ (at IC_{25} dose), with or without trastuzumab (50 or 100 μg/ml) for 72 h. **B**, SKBR3 cells were first treated with hSGZ (at IC_{25} dose) for 6 h, and then 50 μg/ml trastuzumab were added for 72 h (sequence I). Alternatively, cells were pretreated with 50 μg/ml trastuzumab for 6 h, followed by the addition of hSGZ (IC_{25}). The cells were then incubated for a total of 72 h (sequence II). Coexposure hSGZ (at IC_{25} dose) and 50 μg/ml trastuzumab to the cells for 72 h (sequence III). Cell viability was assessed by

crystal violet staining. Statistical significance was calculated using a two-tailed, independent samples t test. n.s., not significant ($p>0.05$).

A

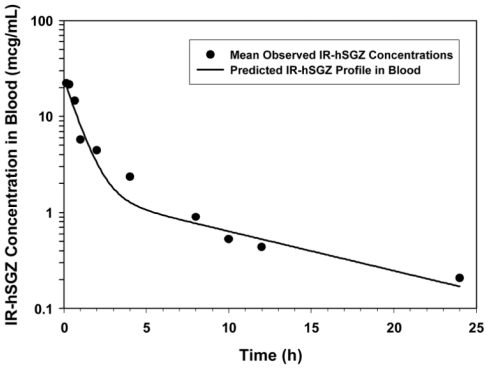

Parameter	value
$t_{1/2\alpha}$ (h)	1.26
$t_{1/2\beta}$ (h)	7.29
C_0 (μg/mL)	24.9
V_d (mL)	3.21
V ss (mL)	12.28
$AUC_{0-\infty}$ (μg*h/mL)	35.83
CL (mL/h)	2.23
MRT	5.50

B

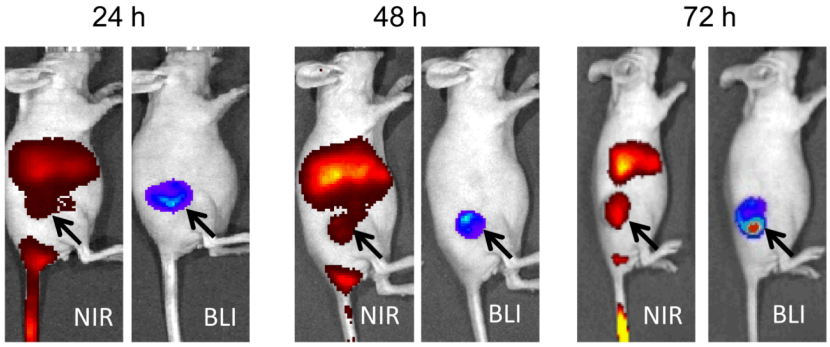

C

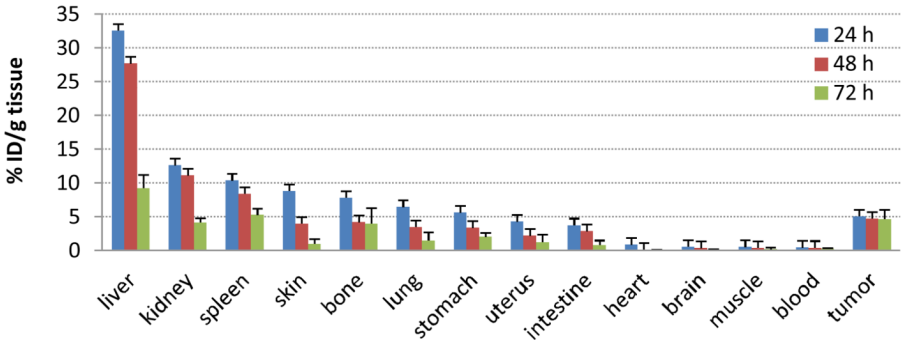

Figure 4.

Pharmacokinetics and biodistibution of IRDye 800CW-labeled hSGZ (IR-hSGZ) in mice. **A**, pharmacokinetic of IR-hSGZ. The IR-hSGZ was injected intravenously into BALB/c mice. Groups of mice (3 mice per group) were sacrificed at various time points after injection. The fluorescent activity in plasma was assessed, and the mean blood concentration–time profile of IR-hSGZ generated using a least squares nonlinear regression. $t_{1/2\alpha}$ and $t_{1/2\beta}$ represent half-lives in initial distribution phase and terminal elimination phase, respectively; C_0 is the estimated initial drug concentration in the blood; Vd is the volume of distribution of central compartment; Vss is volume of distribution at steady state; $AUC_{0-\infty}$ is the area under the

blood concentration versus time curve; CL is total body clearance; and MRT is mean resident time. **B**, whole body imaging results of the nude mice bearing MDA-MB-231/Luc tumors intravenously injected with IR-hSGZ and imaged at 24, 48 and 72 h. The BLI images show only tumor burden. NIR, Near-infrared imaging; BLI, Bioluminescent imaging. Arrow indicates tumor burden. **C**, biodistribution of IR-hSGZ at 24, 48 and 72 h after intravenous injection of IR-hSGZ in nude mice bearing MDA-MB-231/Luc tumors. Data are presented as percentage of injected dose per gram of tissues (%ID/g tissue), represented as mean ± SD (n=5).

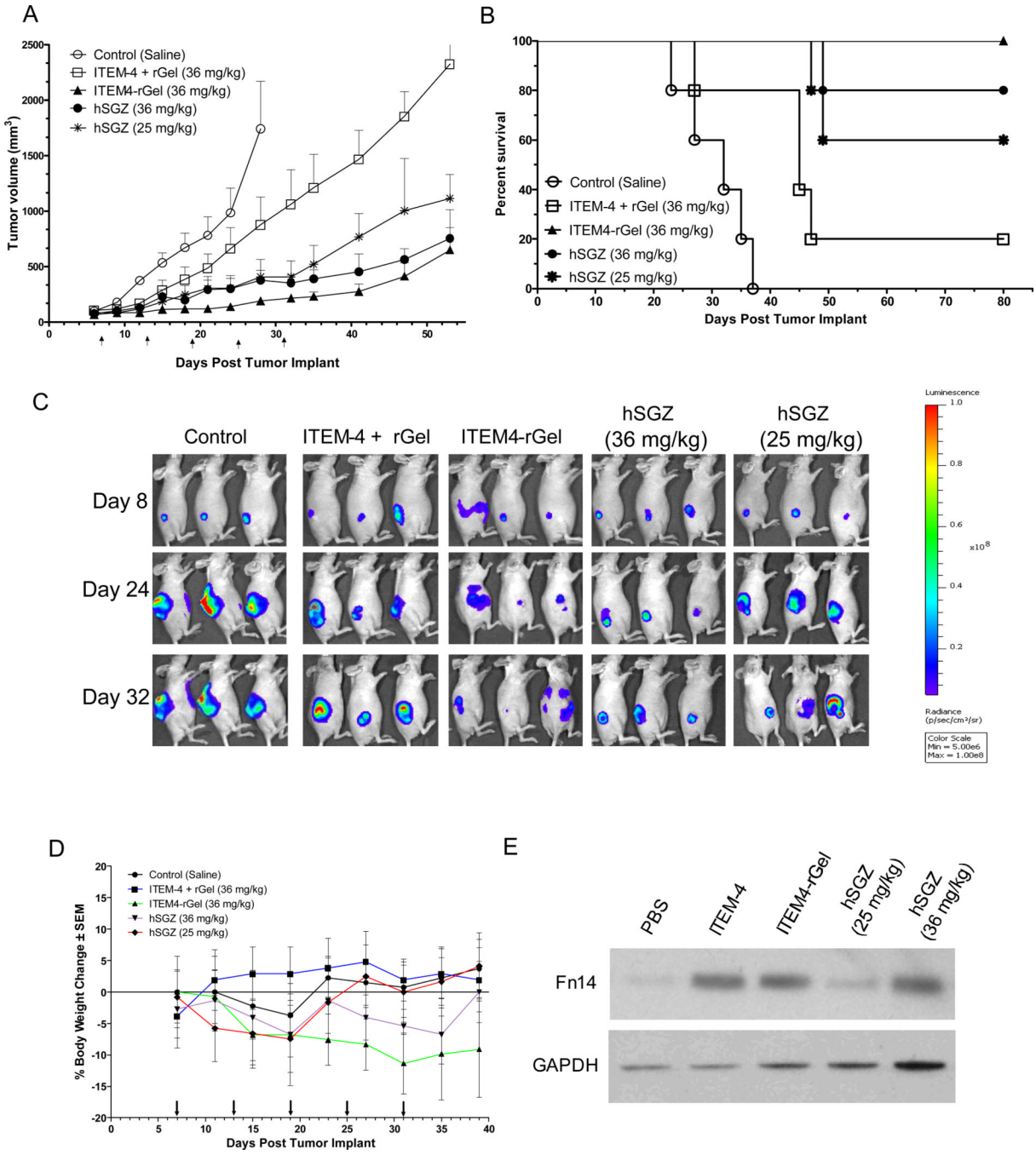

Figure 5.

Both ITEM4-rGel and hSGZ inhibit tumor growth and prolong survival in a MDA-MB-231/Luc breast tumor xenograft model. MDA-MB-231/luc cells were implanted subcutaneously and groups of mice (n = 5) were treated (*i.v.* via tail vein) with saline, ITEM-4 plus rGel, ITEM4-rGel (36 mg/kg), and hSGZ (36 mg/kg and 25 mg/kg) every 6 days starting when the tumors were approximately 100 mm^3. Arrow indicates dosing days. **A**, efficacy data are plotted as mean tumor volume (in mm^3) ± SEM. Tumor size assessed by direct caliper measurement. **B**, survival data are plotted as percent of animals surviving in each group using a predefined cutoff volume of 1,200 mm^3 as a surrogate for survival. **C**, the BLI

images of mice on selected days were shown. **D**, percent change in body weight of each group of mice is plotted as a function of time. **E**, Tumor tissues from the xenograft experiment in (A) were analyzed for Fn14 and GAPDH expression by Western blot.

Table 1

Cytotoxicity of hSGZ on breast cancer cell lines.

Cell lines	Fn14 receptor	HER2 receptor	IC_{50} (nM)			Targeting Index*
			rGel	hSGZ		
eB1	+	++	835	0.1		8, 350
MDA-MB-231	+++	−−	745	0.1		7, 450
SKBr-3	++	+++	1, 550	0.6		2, 538
MCF7/HER2	+++	+++	441	0.7	] p<0.05	630
MCF7	+	−−	452	2.4		188
BT-474/HR	−−	+++	590	489	] n.s	~ 1
BT-474	−−	+++	945	> 489		< 2

*Targeting index represents IC_{50} of rGel/IC_{50} of hSGZ. Student's t test was used to calculate p value. Data are representative of three independent experiments. n.s., not statistically significant (p>0.05).

Table 2

In vitro cytotoxicity of paclitaxel, doxorubicin, ITEM4-rGel, hSGZ and rGel for HeyA8, HeyA8-MDR, MDA-MB-435 and MDA-MB-435/LCC6 ^{MDR1} cells.

Cytotoxic agents	HeyA8-MDR	HeyA8	Resistance fold	MB-435^{MDR1}	MB-435	Resistance fold*
	IC_{50} (nmol/L)			IC_{50} (nmol/L)		
Paclitaxel	70 ± 4	0.07 ± 0.02	1, 000	36.5 ± 13.4	0.006 ± 0.001	6, 083
Doxorubicin	151 ± 5	3.6 ± 3.1	42	796 ± 31.3	45.4 ± 29.4	17
ITEM4-rGel	0.05 ± 0.02	0.05 ± 0.007	1	0.003 ± 0.003	0.007 ± 0.004	0.5
hSGZ	1.8 ± 0.3	1.7 ± 0.3	1	0.008 ± 0.002	0.009 ± 0.007	0.9
rGel	140 ± 57	68 ± 25	2	282 ± 26	270 ± 27	1

The data are presented as the mean IC_{50} ± SD from two independent experiments.

*Resistance fold is defined as IC_{50} of drugs on MDR cells/IC_{50} of drugs on matched parental cells.